Desalination and Water Treatment
www.deswater.com
doi: 10.1080/19443994.2013.814343

52 (2014) 5494–5503
August

Taylor & Francis
Taylor & Francis Group

Removal of Acid Red 299 dye on gold nanoparticles loaded on activated carbon: kinetic and thermodynamic investigation of the removal process

Mehrorang Ghaedi[a,]*, Zahra Andikaey[a], Ali Daneshfar[b], Taybeh Akbari[b], Reza Sahraei[b]

[a]*Chemistry Department, Yasouj University, Yasouj 75918-74831, Iran*
Tel./Fax: (0098) 741 2223048; email: m_ghaedi@mail.yu.ac.ir
[b]*Department of Chemistry, Ilam University, Ilam, Iran*

Received 26 April 2012; Accepted 6 May 2013

ABSTRACT

In this research, the gold (Au) nanoparticles loaded on activated carbon (Au-NP-AC) have been applied for the removal of Acid Red 299 (AR-299). The influence of variables, including the pH, AR-299 concentration, amount of Au-NP-AC, contact time, and temperature in a batch method, on the AR-299 removal has been investigated. Following the optimization variables, by fitting the experimental equilibrium data to Langmuir, Freundlich, and Tempkin, the respective information for each model and their applicability to understand the concept of adsorption was examined. According to R^2 and error analysis, it was found that the adsorption process follows the Langmuir model. It was found that among various kinetic models, such as first- and second-order, Elovich, and intraparticle diffusion model, the experimental data at various removal times was interpreted using the second-order kinetic model with the involvement of the intraparticle diffusion model. The negative value of Gibbs free energy and the positive value of the adsorption enthalpy show the spontaneous and endothermic nature of the adsorption process.

Keywords: Adsorption; Acid Red 299 (AR-299); Gold nanoparticle loaded on activated carbon (Au-NP-AC); Kinetic and thermodynamics of adsorption

1. Introduction

Dyes and color materials produced and/or used in the industry for producing household goods, textile, food, etc. release effluents. Their wastewater containing toxic are hazardous to the environment and aquatic environment, and creates immense toxicity for human health. Dyes, via generation of undesirable coloring to water, are lethal for the aquatic life. Their intermediate and oxidation/reaction products generate toxic and hazardous problems in water. Theses point to the increase in the need for their removal from wastewater [1–3]. Dye removal from wastewater before reuse is essential for the protection of health and environment. Wastewater can be treated using flocculation, coagulation, precipitation, adsorption, membrane filtration, electrochemical techniques, and ozonation [4,5]. The technical and economic feasibility of each technique is determined by the dye type, wastewater composition, operation costs, and generated waste products. Individual application of each

---

*Corresponding author.

technique cannot achieve complete decolorization. Therefore, combination of different techniques is required to cope with the limitations [6–8]. Metallic nanoparticles-based adsorbents have been widely applied for nanoscale devices to bind and coordinate biological materials. Organic monolayer-protected metal nanoparticles are particularly attractive for their chemical stability and quantitative control of functionalization. Azo dyes, especially synthetic ones, are applied in many textile industries [9] with azo group band (–N=N–) due to their low cost, high solubility, and stability. These compounds and their intermediate products are toxic, carcinogenic, and mutagenic to aquatic life [10–12]. Acid dyes (water-soluble anionic dyes) are applied to nylon, wool, silk, and modified acrylics [13–33]. Acid Red 299, (AR-299) with molecular formula of $C_{26}H_{24}N_5NaO_5S$, belongs to pigments/ acid dyes (Fig. 1). In this research, gold nanoparticles loaded on activated carbon (Au-NP-AC) were efficiently applied for the removal of AR-299. Equilibrium adsorption isotherms were investigated and the experimental data were analyzed by Langmuir, Freundlich, Tempkin, Freundlich, and Dubinin–Radushkevich (D–R) isotherm models.

2. Experimental

2.1. Instruments and reagents

AR-299 (CAS number = 12,220-29-0; molar mass = 541.55 g mol^{-1}, λ_{max} = 523 nm) was used throughout experiments using 50 mL capacity glass beaker in a batch method. Stock of AR-299 solution (100 mg L^{-1}) was prepared by dissolving 100 mg of AR-299 in double-distilled water and the test solutions were prepared by diluting stock solution to the desired concentrations daily. The pH measurements were done using pH/ion meter model-686 (Metrohm, Switzerland, Swiss), and absorption studies were carried out using Jusco UV–Visible spectrophotometer model V-570. The pH was adjusted by HCl/KOH. All chemicals, including NaOH, HCl, and KCl, of analytical reagent grade were purchased from Merck, Darmstadt, Germany.

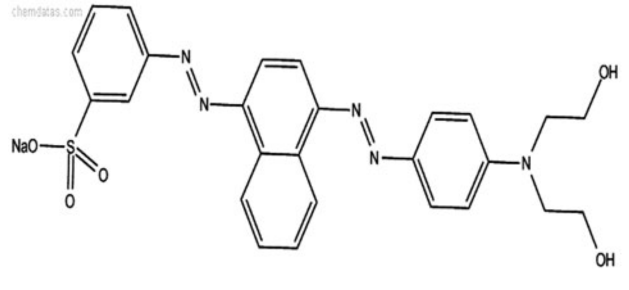

Fig. 1. Chemical structure of AR-299.

2.2. Measurements of dye uptake

Concentrations of AR-299 in the solution were evaluated based on the linear calibration curve obtained at the same conditions. The time dependencies of adsorption in the intervals of 1–45 min show that equilibrium was established after 35 min. The effect of initial pH (pH was adjusted by addition of HCl/KOH) in the range of 2–8 on adsorption was studied at 15 mg L^{-1}. The general AR-299 removal in the range of 5–30 mg L^{-1} dye concentrations at optimum conditions was examined and the amount of adsorbed AR-299 was calculated using the following mass balance relationship:

$$q_e = (C_0 - C_e)V/W \tag{1}$$

where C_0 and C_e are the initial and equilibrium dye concentrations in the solution, respectively (mg L^{-1}), V is the volume of the solution (L), and W is the mass (g) of adsorbent.

2.3. Synthesis of Au-NP-AC

Gold (Au) nanoparticles were synthesized based on reduction of gold ions in aqueous solution [34,35]. In a typical preparation, a 200 μL aliquot of a 0.05 M $HAuCl_4{\cdot}3H_2O$ aqueous solution was added into 50 mL of aqueous solution containing 0.15 wt.% of soluble starch and vigorously stirred for 1 h. The pH of resulting the solution was adjusted to 9.0 by adding 0.05 M of NaOH solution. After about 8 min, the solution turned light pink, which indicated the initial formation of the Au nanoparticles. The mixture was maintained at 70 °C for 40 min and the color of the reaction solution became winy red.

The procedure for the preparation of Au-NP-AC was applied as follows: 500 mL of the freshly prepared Au nanoparticles solution was mixed with activated carbon (25 g) in a 1,000 mL Erlenmeyer flask under magnetic stirring for up to 12 h, resulting in the deposition of the Au nanoparticles on activated carbon. The Au-NP-AC were then filtered and extensively washed with double-distilled water. Filtrate solutions were analyzed for Au nanoparticles using UV–vis spectrophotometry. Au-NP-AC was dried at 110 °C in an oven for 10 h. Then, it was stored in air at room temperature and was found to have a shelf life of at least 1.0 year.

Absorption measurements were carried out on a Perkin Elmer Lambda 25 spectrophotometer using a quartz cell with an optical path of 1 cm. The shape and surface morphology of the Au nanoparticles were investigated by field emission scanning electron microscope (FESEM, Hitachi S4160) under an acceleration voltage of 15 kV. Transmission electron microscope (TEM) samples were prepared by dropping diluted solutions of Au nanoparticles onto 400-mesh carbon-coated copper grids with the excessive solvent immediately getting evaporated. The morphology and electron diffraction (ED) pattern of the Au nanoparticles were determined by a Hitachi H-800 TEM at an operating voltage of 200 kV.

3. Results and discussion

3.1. Characterization of the Au-NP-AC

Fig. 2 shows the UV–Vis absorption spectra obtained at different time intervals after mixing $HAuCl_4 \cdot 3H_2O$ solution with soluble starch solution at 70℃. The formation of the Au nanoparticles in the colloidal solution was monitored from their absorption spectra, as the small noble metal particles exhibit absorption band in the UV–Vis spectral region due to surface plasmon resonance (SPR) [33,35]. The process of reduction of Au^{3+} ions using starch was rapid, yielding a broad absorption band centered at about 520 nm until 8 min of reaction time, which was attributed to the SPR of the Au nanoparticles [36]. The broad band indicates a relatively high polydispersity, both in size and shape of the Au nanoparticles. The intensity of the SPR band increased systematically with the increase in the reaction time and reached a maximum after about 36 min. Thereafter, the intensity of the SPR band did not change. The reduction of Au^{3+} ions with starch aqueous solution at 70℃ leads to the formation of Au nanoparticles that are stable in solution for several months. This indicates that the soluble starch serves as both reducing and protecting agent.

The FE-SEM image of the Au nanoparticles' (Fig. 3) semi-spherical shape and uniform size distribution of Au nanoparticles in the range of 20–70 nm agree with the TEM image (Fig. 4(a)) with relatively narrow particle size distribution (25–65 nm range). The ED rings of the Au nanoparticles (Fig. 4(b)) correspond to the crystalline planes of the cubic structure showing its nanocrystalline nature. The ED pattern in the plane of [1 1 1], [2 0 0], [2 2 0], [3 1 1], and [2 2 2] indicates the crystal planes of face-centered cubic (fcc) lattice structure of the Au nanoparticles [33,37].

3.2. Effect of contact time and initial dye concentration

The variation in AR-299 removal percentage with contact time at 15 mg/L (Fig. 5) shows that the maximum amount of AR-299 removal occurs at the contact time of 35 min and further addition has not significantly changed the removal percentage. At lower initial concentration, the adsorption due to the high ratio of dye molecule to the vacant adsorbent size is very fast, while at higher concentration longer time is required to reach equilibrium. At higher concentration, due to occupation of vacant sites of the adsorbent, the

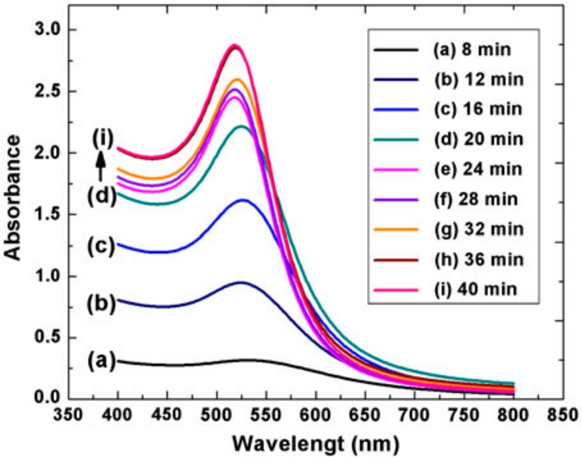

Fig. 2. Temporal evolution of UV–Vis absorption spectra after addition of $HAuCl_4$ solution into soluble starch solution at 70℃.

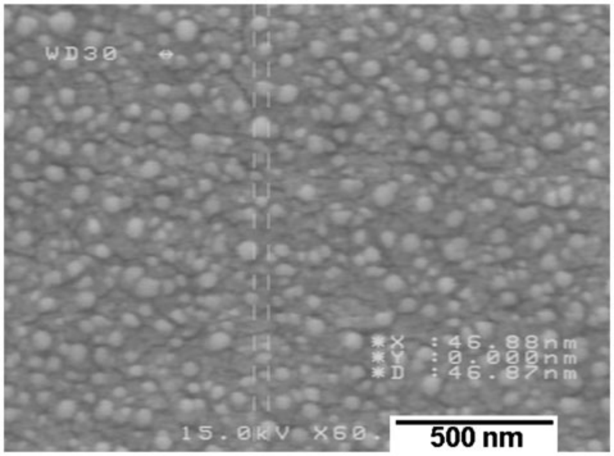

Fig. 3. FESEM image of the Au nanoparticles loaded onto activated carbon.

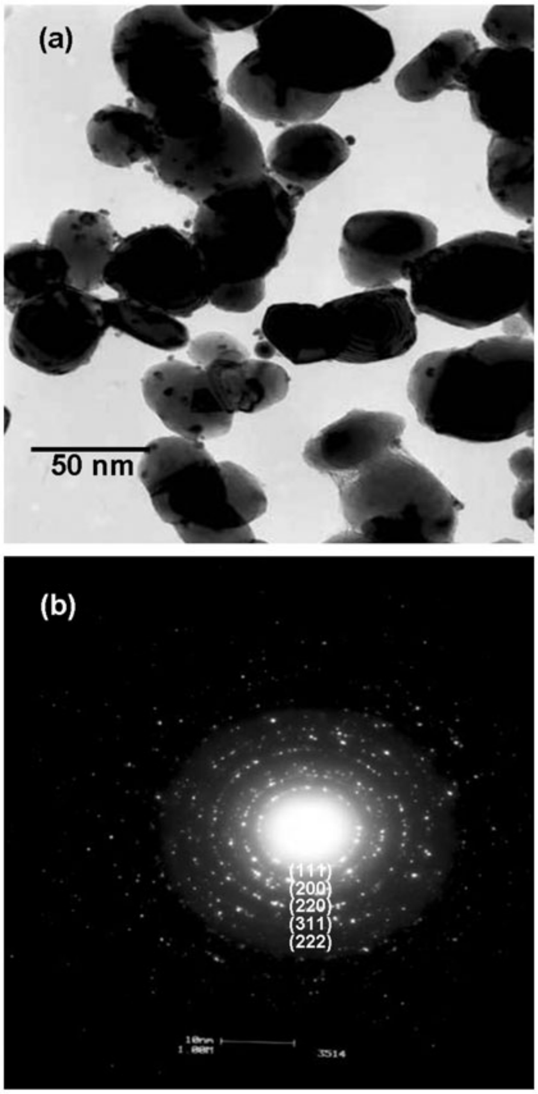

Fig. 4. (a) Typical TEM image of the starch-stabilized Au nanoparticles and (b) the ED pattern of the Au nanoparticles.

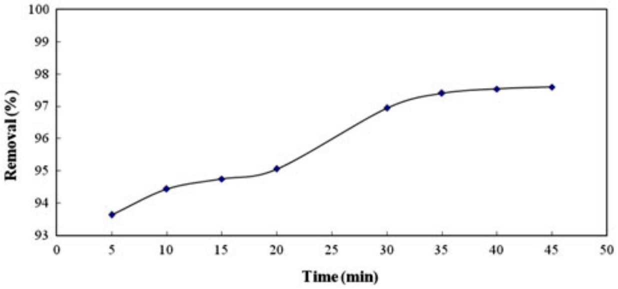

Fig. 5. Effect of contact time of removal of AR-299 on Au-NP-AC.

adsorption process rate slows down and more adsorption time is required to achieve equilibrium [38].

3.3. Effect of pH

The pH, via affecting the adsorbent surface charge and degree of ionization of dye functional group, subsequently leads to the shift in reaction kinetics and equilibrium characteristics of the adsorption process. It is common observation that the anions adsorption is favorable at lower pH via electrostatic force, and due to negative surface charge the cations adsorption occurs at higher pH. Consequently, the dye molecule has high positively charged density at low pH, while at pH_0 below 3, due to electrostatic repulsion between the positive charge adsorbent surface and the dye molecule, the removal percentage significantly decreased. With rising pH, both the adsorbent surface and dye molecule get neutralized and via different mechanisms, such as hydrogen bonding, soft–soft interaction (with gold nanoparticle), and π–π interaction with AC as backbone, the removal percentage significantly increased. At higher pH, probably both the adsorbent and AR-299 get negatively charged and, due to repulsion, the removal percentage significantly decreased (Fig. 6) [39,40].

3.4. Effect of adsorbent dose

The AR-299 removal percentage on Au-NP-AC was studied at different adsorbent amounts in the range of 0.04 g at 15 mg/L AR-299 concentration, pH (5), and (30 ± 1˚C) at 45 min. As it is observed (Fig. 7), by raising the amount of adsorbent till 1.2 g/L, due to the increase in the number of vacant sites and diffusion (driving force of adsorption), the rate of AR-299 transfer to the adsorbent surface significantly increased. The removal percentage increased from 65.1 to 99.9% as the amount of adsorbent increased from 0.5 to 1.2 g/L. The adsorption capacity decreased

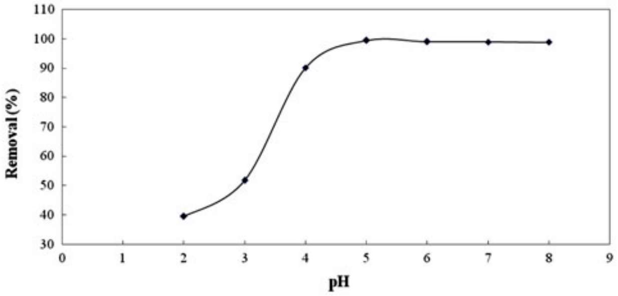

Fig. 6. Effect of pH on the removal of AR-299 at room temperature on Au-NP-AC.

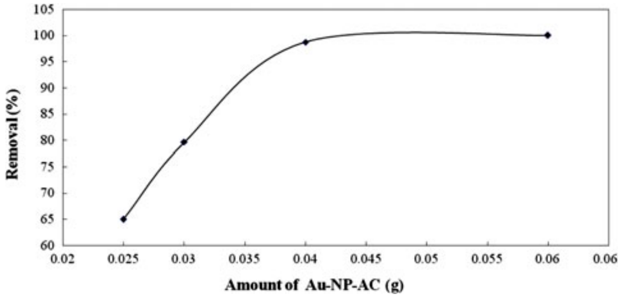

Fig. 7. Effect of amount of adsorbent (g) on AR-299 removal at room temperature on Au-NP-AC.

significantly with the increase in the adsorbent dosage [41,42].

3.5. *Effect of ionic strength*

Another parameter affecting the removal percentage is the typical wastewater contaminants [43]. It is well known that additives, such as, salts either accelerate or retard the dye adsorption processes. Salts via affecting the electrostatic interaction, enhance the degree of dissociation of the dye molecules and facilitate or retard the amount of adsorbed pollutant. The dominant nature of the first role confirms that adsorption occurs through electrostatic interaction, especially for charged adsorbate and adsorbent [44–48].

3.6. *Adsorption isotherm*

It is necessary to establish the most appropriate correlations for the equilibrium data using conventional isotherm models like Langmuir, Freundlich, Tempkin, and Dubinin–Radushkevich.

Applicability of the isotherm equations was compared by judging the correlation coefficients, (R^2) and error analysis.

$$\text{Langmuir: } C_e/q_e = 1/(K_L q_m) + (1/q_m)C_e \tag{2}$$

$$\text{Freundlich: } q_e = K_F C_e{}^{1/n} \tag{3}$$

K_L is a direct measurement of the adsorption intensity related to the heat of adsorption (dm mg^{-1}) and q_m is the maximum amount of adsorbed analytes. The q_m and K_L values can be determined from the slope and intercept of the respective lines obtained by plotting log C_e/q_e vs. C_e. In Eq. (3), K_F (constant related to the bonding energy) represents the quantity of dye adsorbed onto the adsorbent. The slope $1/n$ (between 0 and 1) is a measure of adsorption intensity or surface heterogeneity [49–51]. The value below one indicates a normal Freundlich isotherm, while respective values higher than one indicate cooperative adsorption [52]. A plot of Ln q_e vs. C_e enables the empirical constants, K_F and $1/n$, to be determined from the intercept and slope of the linear regression.

As can be seen from Table 1, the results of Langmuir and Freundlich isotherms fit the AR-299 removal by the proposed adsorbent and follow the Langmuir model (better fit as reflected by correlation coefficients (R^2) of 0.997) with monolayer adsorption capacity ($Q_m = 20\,\text{mg g}^{-1}$) of $1/n$ of 0.540 indicating favorable adsorption [52–58].

Tempkin and Pyzhev [59] assume that the adsorption heat in each layer decreases linearly with surface coverage of adsorbent due to sorbate–adsorbate interactions. The linear form of the Tempkin isotherm equation is represented by the following equation [60]:

$$q_e = B_1 \ln K_T + B_1 \ln C_e \tag{4}$$

Values of B_1 and K_T were calculated from the plot of q_e against ln C_e (Table 1). Tempkin isotherm, with a relatively high correlation coefficient ($R^2 > 0.98$), is near the value of Langmuir.

The Dubinin–Radushkevich (D–R) isotherm is applied to estimate the porosity of apparent free energy and the characteristics of adsorption [61,62], and its linear form can be shown in the following equation:

$$\ln q_e = \ln Q_m - K\varepsilon^2 \tag{5}$$

where ε (Polanyi potential) can be calculated from Eq. (5):

$$\varepsilon = RT \ln(1 + 1/C_e) \tag{6}$$

From the plot slope (ln q_e vs. ε^2) K (mol^2 (kJ^2) $^{-1}$) and the intercept yields, the adsorption capacity (Q_m (mg g^{-1})) can be calculated simply. The mean free energy of adsorption (E) calculated from the K value is based on the following equation [63]:

$$E = 1/(2K)^{1/2} \tag{7}$$

The calculated D–R constants for the adsorption of AR-299 on Au-NP-AC (Table 1) show that the model correlation coefficient is much lower than other defined isotherms values.

3.7. *Kinetic studies*

The behavior of the AR-299 adsorption is analyzed using first- and second-order kinetic models and intraparticle diffusion model [64].

Table 1
Isotherm constant parameters and correlation coefficients calculated for various adsorption dye onto adsorbent

Isotherm	Equation	Plot	Parameters	Adsorbent Au-NP-AC
Langmuir 2	$1/q_e = 1/(K_a Q_m C_e) + 1/Q_m$	A plot of C_e/q_e vs. C_e should indicate a straight line of slope $1/Q_m$ and an intercept of $1/(K_a Q_m)$	Q_m (mg/g)	20
			K_a (L mg^{-1})	0.355
			R^2	0.997
Freundlich	$\ln q_e = \ln K_F + (1/n) \ln C_e$	The values of K_f and $1/n$ were determined from the intercept and slope of linear plot of ln q_e vs. ln C_e, respectively	$1/n$	0.540
			K_F (L/mg)	5.124
			R^2	0.995
Tempkin	$q_e = B_1 \ln K_T + B_1 \ln C_e$	Values of B_1 and K_T were calculated from the plot of q_e against ln C_e	B_1	4.840
			K_T (L/mg)	2.920
			R^2	0.986
Dubinin and Radushkevich (D–R)	$\ln q_e = \ln Q_s - B\varepsilon^2$	The slope of the plot of ln q_e vs. ε^2 gives K (mol^2 (kJ^2) $^{-1}$) and the intercept yields the adsorption capacity, Q_m (mg g^{-1})	Q_s (mg/g)	13.805
			B	3E-07
			E (kJ/mol) = $1/(2B)^{1/2}$	1,291
			R^2	0.898

Table 2
Kinetic parameters for the adsorption of AR-299 onto Au NP- AC adsorbent

Model	Equation	Plot	Parameters	Adsorbent Au-NP-AC
First-order kinetic	$\text{Log}\ (q_e - q_t) = \log (q_e) - (k_1/2.303)t$	Plot the values of log $(q_e - q_t)$ vs. t to give a linear relationship from which k_1 and q_e can be determined from the slope and intercept, respectively	k_1	0.074
			q_e (calc)	1.346
			R^2	0.915
Second-order kinetic	$(t/q_t)=1/(k_2 {q_e}^2)+1/q_e(t)$	Plot the values of (t/q_t) versus t to give a linear relationship from which k_1 and q_e can be determined from the slope and intercept, respectively	k_2	0.122
			q_e (calc)	18.518
			R^2	0.999
Intraparticle diffusion	$q_t = K_{dif}\, t^{1/2} + C$	The values of K_{dif} and C were calculated from the slopes of q_t vs. $t^{1/2}$	K_{diff}	0.177
			C	17.12
			R^2	0.959
Elovich	$q_t = 1/\beta \ln(\alpha\beta) + 1/\beta \ln(t)$	Plot the values of (q_t) vs. ln(t) to give a linear relationship from which α and β can be determined from the slope and intercept, respectively	β	2.762
			R^2	0.917
Experimental data			q_e (exp)	18.289

A linear form of the first-order model expression is:

$$\log(q_e - q_t) = \log q_e - (k_1 t/2.303)t \tag{8}$$

where q_e and q_t (mg g^{-1}) are the amounts adsorbed at equilibrium and time t (min), respectively, and k_1 (min^{-1}) is the rate constant of Langergren first-order adsorption (min^{-1}).

The kinetic data are further analyzed using the pseudo-second-order kinetics expressed as:

$$t/q_t = (1/k_2 q_e^2) + (1/q_e)t \tag{9}$$

where k_2 (g·mg^{-1} min^{-1}) is the rate constant of pseudo-second-order adsorption. If the second-order kinetics is applicable, the plot of t/q_t vs. t should give a linear relationship.

The adsorbate species are most probably transported from the bulk of the solution into the solid phase with an intraparticle diffusion process. The possibility of intraparticle diffusion is explored by using the intraparticle diffusion model [65] as follows:

$$q_t = k_{id} t^{1/2} + C \tag{10}$$

where C is the intercept and k_{id} is the intraparticle diffusion rate constant. The values of k_{id} and C and the corresponding linear regression correlation coefficient (R^2) are given in Table 2. The intraparticle rate constants calculated are 0.177 mg·g^{-1}·min$^{-1/2}$ for AR-299 onto Au-NP-AC [66,67].

3.8. Thermodynamic study

Thermodynamic parameters generally required to confirm the nature of adsorption and can be obtained from the following Equations:

$$\Delta G^\circ = -RT \ln K_c \tag{11}$$

Values of K_c may be calculated from the relation $K_c = (q_e/C_e)$ at different temperatures and extrapolating to zero. The calculated thermodynamic parameters (Table 3) show negative ΔG° values (spontaneous nature and feasibility of the adsorption process), and a more negative value with the increase in temperature from 283 to 333 K implies the favorability of adsorption at higher temperature. The result also shows an increase in the values of $T\Delta S^\circ$ with elevating temperature $|\Delta H^\circ| < |T\Delta S^\circ|$ indicating that the adsorption process is dominated by entropy rather than enthalpy changes [68].

The values of enthalpy (ΔH°) and entropy change (ΔS°) may be determined from the slope and intercept of plots of ln Kc vs. $1/T$ in van't Hoff equation (Fig. 8) as follows:

$$\ln Kc = \Delta S^\circ/R - \Delta H^\circ/RT \tag{12}$$

Also, ΔG° can be obtained from ΔH° and ΔS° evaluated from van't Hoff equation at each temperature by means of the equation below:

$$\Delta G^\circ = \Delta G^\circ - T\Delta S^\circ \tag{13}$$

The positive values of ΔH° confirm the endothermic nature of the adsorption process, while the positive ΔS° values suggest the increase in the adsorbate concentration in solid–liquid interface. To further support the assertion that physical adsorption is the predominant mechanism, the values of activation energy (E_a) and sticking probability (S^*) were estimated from the experimental and that surface coverage was calculated (θ) [69] as follows:

$$S^* = (1-\theta)e^{(-Ea/RT)} \tag{14}$$

and can be linearized as follows from Eq. (15):

Table 3
Thermodynamic parameters for the adsorption of AR-299 onto Au NP-AC

Parameters	C_0 (mg/L)	Temperature, K				
		283.15	293.15	313.15	323.15	333.15
AR-299	k_c	2.372	2.464	12.474	12.877	15.226
	ΔG^0 J/mol	−2033	−2,197	−6,570	−6,865	−7,542
Parameters	AR-299 onto Au NP-AC					
ΔS^0 (J/mol K)	126.207					
ΔH^0 (kJ/mol)	33.979					
E_a, kJ/mol	28.608					
S^*	1.743E-06					

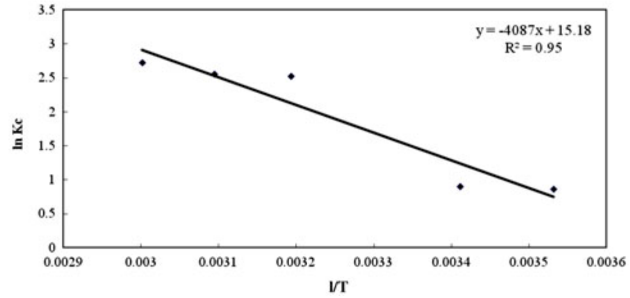

Fig. 8. $\ln K_c$ vs. $1/T$ in the van't Hoff equation.

$$\ln(1-\theta) = \mathrm{Ln}S^* + E_a/RT \tag{15}$$

The sticking probability (S^*) value lies in the range $0 < S^* < 1$ depending on the system temperature.

The parameter (S^*) indicates the measure of the potential of an adsorbate to remain on the adsorbent. The surface coverage (θ) can be calculated from the following equation:

$$\theta = [1 - C_e/C_o] \tag{16}$$

The activation energy and sticking probability were estimated from the slope and intercept of plot of Ln $(1-\theta)$ vs. $1/T$. Activated energy for adsorption of $15\,\mathrm{mg\,L^{-1}}$ AR-299 concentration was found to be $28.6\,\mathrm{mg\,L^{-1}}$ on the Au-NP-AC.

The positive values of E_a indicate the endothermic nature of the adsorption process.

4. Conclusion

An adsorption experiment of AR-299 under different experimental conditions in a batch mode has been conducted and the influence of variables, such as the amount of adsorbent, AR-299 concentration, contact time, and pH of the solution, on its removal percentage was investigated. Higher dye removal was found within 35 min of the start of every experiment that under the optimum experimental pH of 5–7. The proposed adsorption system has the following atributes:

(1) The removal process follows the Langmuir model with maximum adsorption capacity of $20\,\mathrm{mg\,g^{-1}}$.
(2) The rate of AR-299 from bulk to the adsorbent surface follows the pseudo-second-order kinetic model with the involvement of the interparticle diffusion model.
(3) Using asmall amount of Au-NP-AC, higher amounts (0.04 g) and removal percentages (higher of 99%) for the AR-299 can be obtained in a short time (35 min).

Abbreviations

C_0	—	initial adsorbate concentration, mg/L
C_e	—	equilibrium adsorbate concentration, mg/L
K_F	—	empirical constants depend to several environmental factors, $(\mathrm{mg\ g^{-1}})\ (\mathrm{L\ mg^{-1}})^{1/n}$
K_L	—	Langmuir constant related with affinity of the points of union ($\mathrm{L\ mg^{-1}}$)
n	—	empirical parameter representing the energetic heterogeneity of the adsorption sites
Q^o	—	maximum adsorption capacity corresponding to complete monolayer coverage ($\mathrm{mg\ g^{-1}}$)
q_e	—	adsorption capacity at equilibrium solute concentration (C ($\mathrm{mg\ g^{-1}}$))
R^2	—	correlation coefficient
V	—	volume of solution (L)
W	—	weight of adsorbent (g)
k_1	—	rate constant of pseudo-first-order adsorption ($\mathrm{min^{-1}}$)
k_2	—	second-order rate constant of adsorption ($\mathrm{g\ mg^{-1}min^{-1}}$)
h	—	second-order rate constants ($\mathrm{mg\ g^{-1}\ min^{-1}}$)
$ß$	—	desorption constant ($\mathrm{g\ mg^{-1}}$)
ΔG°	—	free energy change ($\mathrm{kJ\ mol^{-1}}$)
ΔH°	—	heat of adsorption ($\mathrm{kJ\ mol^{-1}}$)
ΔS°	—	standard entropy ($\mathrm{kJ\ mol^{-1}\ K^{-1}}$)
K_c	—	thermodynamic equilibrium constant
E_a	—	activation energy of adsorption ($\mathrm{kJ\ mol^{-1}}$)
S^*	—	sticking probability indicates the measure of the potential of an adsorbate to remain on the adsorbent in definite
θ	—	surface coverage

References

[1] N. Daneshvar, M. Ayazloo, A.R. Khataee, Biological decolorization of dye solution containing malachite green by microalgae *Cosmarium* sp, Bioresour. Technol. 98 (2007) 1176–1182.

[2] P. Nigam, G. Armour, I.M. Banat, Physical removal of textile dyes from effluents and solid-state fermentation of dye-adsorbed agricultural residues, Bioresour. Technol. 72 (2000) 219–226.

[3] A. Mittal, D. Kaur, J. Mittal, Applicability of waste materials-bottom ash and deoiled soya-as adsorbents for the removal and recovery of a hazardous dye, brilliant green, J. Coll. Interf. Sci. 326 (2008) 8–17.

[4] A. Dabrowski, Adsorption-from theory to practice, Adv. Coll. Interf. 93 (2001) 135–224.

[5] N. Hoda, E. Bayram, E. Ayranci, Kinetic and equilibrium studies on the removal of acid dyes from aqueous solutions by adsorption onto activated carbon cloth, J. Hazard. Mater. B 137 (2006) 344–351.

[6] D. Suteu, D. Bilba, Equilibrium and kinetic study of reactive dye brilliant red HE-3B adsorption by activated charcoal, Acta Chim. Slov. 52 (2005) 73–79.

[7] M. Ghaedi, A. Hassanzadeh, S. Nasiri Kokhdan, Multiwalled carbon nanotubes as adsorbents for the kinetic and equilibrium study of the removal of alizarin red S and morin, J. Chem. Eng. Data 56 (2011) 2511–2520.

[8] M. Ghaedi, B. Sadeghian, S.N. Kokhdan, A.A. Pebdani, R. Sahraei, A. Daneshfar, A. Mihandoost, Study of removal of Direct Yellow 12 by cadmium oxide nanowires loaded on activated carbon, Mater. Sci. Eng. C 33(4) (2013) 2258–2265.

[9] J.C. Garcia, J.I. Simionato, A.E.C. de Silva, J. Nozaki, N.E. de Souza, Solar Energy 83 (2009) 316–322.

[10] M.B. Kasiri, H. Aleboyeh, A. Aleboyeh, Degradation of acid blue 74 using Fe-ZSM5 zeolite as a heterogeneous photo-Fenton catalyst, Appl. Catal. B: Environ. 84 (2008) 9–15.

[11] S. Renganathan, W.R. Thilagaraj, L.R. Miranda, P. Gautam, M. Velan, Accumulation of acid orange 7, Acid Red 18 and reactive black 5 by growing Schizophyllum commune, Bioresour. Technol. 97 (2006) 2189–2193.

[12] R. Shokoohi, V. Vatanpoor, M. Zarrabi, A. Vatani, Adsorption of Acid Red 18 (AR18) by activated carbon from poplar wood – A kinetic and equilibrium study, E-J. Chem. 7 (2010) 65–72.

[13] W.T. Tsai, C.W. Lai, K.J. Hsien, The effects of pH and salinity on kinetics of paraquat sorption onto activated clay, Coll. Surf. A 224 (2003) 99–105.

[14] A. Duran, M. Tuzen, M. Soylak, Preconcentration of some trace elements via using multiwalled carbon nanotubes as solid phase extraction adsorbent, J. Hazard. Mater. 169 (2009) 466–471.

[15] M. Tuzen, K.O. Saygi, C. Usta, M. Soylak, *Pseudomonas aeruginosa* immobilized multiwalled carbon nanotubes as biosorbent for heavy metal ions, Bioresour. Technol. 99 (2008) 1563–1570.

[16] M. Tuzen, K.O. Saygi, M. Soylak, Solid phase extraction of heavy metal ions in environmental samples on multiwalled carbon nanotubes, J. Hazard. Mater. 152 (2008) 632–639.

[17] M. Tuzen, M. Soylak, Multiwalled carbon nanotubes for speciation of chromium in environmental samples, J. Hazard. Mater. 147 (2007) 219–225.

[18] M.H. Habibi, M. Mikhak, Synthesis of nanocrystalline zinc titanate ecandrewsite by sol–gel: Optimization of heat treatment condition for red shift sensitization, Curr. Nanosci. 7 (2011) 603–607.

[19] M.H. Habibi, R. Mokhtari, Novel sulfur-doped niobium pentoxide nanoparticles: Fabrication, characterization, visible light sensitization and redox charge transfer study, J. Sol-Gel Sci. Technol. 59 (2011) 352–357.

[20] M.H. Habibi, M. Zendehdel, Synthesis and characterization of titania nanoparticles on the surface of microporous perlite using sol–gel method: Influence of titania precursor on characteristics, J. Inorg. Organomet. Polym. 21 (2011) 634–639.

[21] M.H. Habibi, R. Kamrani, R. Mokhtari, Fabrication and characterization of copper nanoparticles using thermal reduction: The effect of nonionic surfactants on size and yield of nanoparticles, Microchim. Acta. 171 (2010) 91–95.

[22] M.H. Habibi, M. Zendehdel, Fabrication and characterization of self-assembled multilayer nanostructure titania with high preferential (101) orientation on alumina thin films by layer-by-layer dip-coating method, Curr. Nanosci. 6 (2010) 642–647.

[23] M.H. Habibi, R. Sheibani, Preparation and characterization of nanocomposite ZnO–Ag thin film containing nano-sized Ag particles: Influence of preheating, annealing temperature and silver content on characteristics, J. Sol-Gel Sci. Technol. 54 (2010) 195–202.

[24] J.A. Baig, T.G. Kazi, L. Elci, Biosorption characteristics of indigenous plant material for trivalent arsenic removal from groundwater: Equilibrium and kinetic studies, Sep. Sci. Technol. 7 (2012) 1044–1054.

[25] J.A. Baig, T.G. Kazi, A.Q. Shah, G.A. Kandhro, H.I. Afridi, S. Khan, Bio-sorption studies on powder of stem of *Acacia nilotica*: Removal of arsenic from surface water, J. Hazard. Mater. 178 (2010) 941–948.

[26] M. Ghaedi, M. Nejati Biyareh, S. Nasiri Kokhdan, S.H. Shamsodini, R. Sahraei, A. Daneshfar, S. Shahriyara, Comparison of the efficiency of palladium and silver nanoparticles loaded on activated carbon and zinc oxide nanorods loaded on activated carbon as new adsorbents for removal of Congo red from aqueous solution: Kinetic and isotherm study, Mater. Sci. Eng. C 32 (2012) 725–734.

[27] M. Ghaedi, H. Khajesharifi, A. Hemmati Yadkuri, M. Roosta, R. Sahraei, A. Daneshfar, Cadmium hydroxide nanowire loaded on activated carbon as efficient adsorbent for removal of bromocresol green, Spectrochim. Acta Part A: Mol. Biomol. Spectrosc. 86 (2012) 62–68.

[28] F. Marahel, M. Ghaedi, S. Nasiri Kokhdan, Silver nanoparticle loaded on activated carbon as an adsorbent for the removal of Sudan red7B from aqueous solution, Fresen. Environ. Bull. 21 (2012) 163–170.

[29] M. Ghaedi, Sh. Heidarpour, S. Nasiri Kokhdan, R. Sahraie, A. Daneshfar, B. Brazesh, Comparison of silver and palladium nanoparticles loaded on activated carbon for efficient removal of methylene blue: Kinetic and isotherm study of removal process, Powder Technol. 228 (2012) 18–25.

[30] F. Marahel, M. Ghaedi, M. Montazerozohori, M. Nejati Biyareh, S. Nasiri Kokhdan, M. Soylak, Solid-phase extraction and determination of trace amount of some metal ions on duolite XAD 761 modified with a new Schiff base as chelating agent in some food samples, Food Chem. Toxicol. 49 (2011) 208–214.

[31] F. Taghizadeh, M. Ghaedi, K. Kamali, E. Sharifpour, R. Sahraie, M.K. Purkait, Comparison of nickel and/or zinc selenide nanoparticle loaded on activated carbon as efficient adsorbents for kinetic and equilibrium study of removal of Arsenazo (III) dye, Powder Technol. 245 (2013) 217–226.

[32] M. Ghaedi, B. Sadeghian, A. Amiri Pebdani, R. Sahraei, A. Daneshfar, C. Duran, Kinetics, thermodynamics and equilibrium evaluation of direct yellow 12 removal by adsorption onto silver nanoparticles loaded activated carbon, Chem. Eng. J. 187 (2012) 133–141.

[33] G. Karimipour, M. Ghaedi, R. Sahraei, A. Daneshfar, M. Nejati Biyareh, Modification of gold nanoparticle loaded on activated carbon with bis(4-methoxysalicylaldehyde)-1,2-phenylenediamine as new sorbent for enrichment of some metal ions, Biol. Trace Element Res. 145 (2012) 109–117.

[34] M.H. Majles Ara, Z. Dehghani, R. Sahraei, A. Daneshfar, Z. Javadi, F. Divsar, Diffraction patterns and non-linear optical properties of gold nanoparticles, J. Quant. Spectrosc. Radiat. Transfer 113 (2012) 366–372.

[35] H. Huang, X. Yang, Synthesis of polysaccharide-stabilized gold and silver nanoparticles: A green method, Carbohydr. Res. 339 (2004) 2627–2631.

[36] S. Link, M.A. El-Sayed, Size and temperature dependence of the Plasmon absorption of colloidal gold nanoparticles, J. Phys. Chem. B 103 (1999) 4212–4217.

[37] M. Brust, J. Fink, D. Bethell, J.D. Schiffrin, C. Kiely, Synthesis and reactions of functionalised gold nanoparticles, J. Chem. Soc. Chem. Commun. 16 (1995) 1655–1656.

[38] B.K. Nandi, A. Goswami, M.K. Purkait, Adsorption characteristics of brilliant green dye on kaolin, J. Hazard. Mater. 161 (2009) 387–395.

[39] C. Namasivayam, D. Prabha, M. Kumutha, Removal of direct red and acid brilliant blue by adsorption on to banana pith, Bioresour. Technol. 64 (1998) 77–79.

[40] I.D. Mall, V.C. Srivastava, N.K. Agarwal, I.M. Mishra, Adsorptive removal of malachite green dye from aqueous solution by bagasse fly ash and activated carbon-kinetic study and equilibrium isotherm analyses, Colloids Surf. A 264 (2005) 17–28.

[41] V.K. Garg, R. Gupta, A.B. Yadav, R. Kumar, Dye removal from aqueous solution by adsorption on treated sawdust, Bioresour. Technol. 89 (2003) 121–124.

[42] H. Lata, V.K. Garg, R.K. Gupta, Adsorptive removal of basic dye by chemically activated Parthenium biomass: Equilibrium and kinetic modeling, Desalination 219 (2008) 250–261.

[43] M.N.V.R. Kumar, A review of chitin and chitosan applications, React. Funct. Polym. 46 (2000) 1–27.

[44] M.S. Chiou, H.Y. Li, Adsorption behavior of reactive dye in aqueous solution on chemical cross-linked chitosan beads, Chemosphere 50 (2003) 1095–1105.

[45] B. Martel, M. Devassine, G. Crini, M. Weltrowski, M. Bourdonneau, M. Morcellet, Preparation and adsorption properties of a beta-cyclodextrin-linked chitosan derivative, J. Polym. Sci. A: Polym. Chem. 39 (2001) 169–176.

[46] K. Miyata, C. Jin, M. Maekawa, Adsorption removal of anionic dyes in wastewater from dyeing by chitosan, Sen'I Gakkaishi 58 (2002) 462–465.

[47] Y. Shimizu, A. Taga, H. Yamaoka, Synthesis of novel crosslinked chitosans with a higher fatty diacid diglycidyl and their adsorption abilities toward acid dyes, Adsorpt. Sci. Technol. 21 (2003) 439–449.

[48] G. Crini, P.-M. Badot, Application of chitosan, a natural aminopolysaccharide, for dye removal from aqueous solutions by adsorption processes using batch studies: A review of recent literature, Prog. Polym. Sci. 33 (2008) 399–447.

[49] K.E. Noll, V. Gounaris, W.S. Hou, Adsorption Technology for Air and Water Pollution Control, Lewis, Chelsea, MI, 1992.

[50] B. Al Duri, G. McKay, Use of Adsorbents for the Removal of Pollutants from Wastewaters, CRC Press, Boca Raton, FL, 1996.

[51] F. Haghseresht, G. Lu, Adsorption characteristics of phenolic compounds onto coal-reject-derived adsorbents, Energy Fuels 12 (1998) 1100–1107.

[52] K. Fytianos, E. Voudrias, E. Kokkalis, Sorption–desorption behaviour of 2,4-dichlorophenol by marine sediments, Chemosphere 40 (2000) 3–6.

[53] W.T. Tsai, M.F. Hsieh, H.F. Sun, S.F. Chien, H.P. Chen, Adsorption of paraquat onto activated bleaching earth, Bull. Environ. Contam. Toxicol. 69 (2002) 189–194.

[54] W.T. Tsai, C.W. Lai, K.J. Hsien, Effect of particle size of activated clay on the adsorption of paraquat from aqueous solution, J. Coll. Interf. Sci. 263 (2003) 29–34.

[55] M. Ghaedi, S. Zamani Amirabad, F. Marahel, S. Nasiri Kokhdan, R. Sahraei, A. Daneshfar, Synthesis and characterization of cadmium selenide nanoparticles loaded on activated carbon and its efficient application for removal of muroxide from aqueous solution, Spectrochim. Acta Part A 83 (2011) 46–51.

[56] M. Ghaedi, H. Tavallali, M. Sharifi, S. Nasiri Kokhdan, A. Asghari, Preparation of low cost activated carbon from *Myrtus communis* and pomegranate and their efficient application for removal of Congo red from aqueous solution, Spectrochim. Acta Part A 86 (2012) 107–114.

[57] W.T. Tsai, C.Y. Chang, M.C. Lin, S.F. Chien, H.F. Sun, M.F. Hsieh, Adsorption of acid dye onto activated carbons prepared from agricultural waste bagasse by $ZnCl_2$ activation, Chemosphere 45 (2001) 51–58.

[58] W.T. Tsai, C.Y. Chang, C.H. Ing, C.F. Chang, Adsorption of acid dyes from aqueous solution on activated bleaching earth, J. Coll. Interf. Sci. 275 (2004) 72–78.

[59] M.J. Tempkin, V. Pyzhev, Kinetics of ammonia synthesis on promoted iron catalysis, Acta Physiochim. URSS 12 (1940) 327–356.

[60] F. Colak, N. Atar, A. Olgun, Biosorption of acidic dyes from aqueous solution by Paenibacillus macerans: Kinetic, thermodynamic and equilibrium studies, Chem. Eng. J. 150 (2009) 122–130.

[61] M.M. Dubinin, Modern state of the theory of volume filling of micropore adsorbents during adsorption of gases and steams on carbon adsorbents, Zh. Fiz. Khim. 39 (1965) 1305–1317.

[62] L.V. Radushkevich, Potential theory of sorption and structure of carbons, Zh. Fiz. Khim. 23 (1949) 1410–1420.

[63] G.C. Panda1, S.K. Das1, A.K. Guha, Jute stick powder as a potential biomass for the removal of congo red and rhodamine B from their aqueous solution, J. Hazard. Mater. 164 (2009) 374–379.

[64] C. Namasivayam, R.T. Yamuna, Adsorption of direct red 12 B by biogas residual slurry: Equilibrium and rate processes, Environ. Pollut. 89 (1995) 1–7.

[65] Y. Bulut, H. Aydin, A kinetics and thermodynamics study of methylene blue adsorption on wheat shells, Desalination 194 (2006) 259–267.

[66] V.K. Gupta, I. Ali, Utilisation of bagasse fly ash (a sugar industry waste) for the removal of copper and zinc from wastewater, Sep. Purif. Technol. 18 (2000) 131–140.

[67] L. Zhuannian, Z. Anning, W. Guirong, Z. Xiaoguang, Adsorption behavior of methyl orange onto modified ultrafine coal powder, Chinese J. Chem. Eng. 17 (2009) 942–948.

[68] M. Ghaedi, M. Ghayedi, S.N. Kokhdan, R. Sahraei, A. Daneshfar, Palladium, silver, and zinc oxide nanoparticles loaded on activated carbon as adsorbent for removal of bromophenol red from aqueous solution, J. Ind. Eng. Chem. 19 (4) (2013) 1209–1217.

[69] N.K. Amin, Removal of direct blue-106 dye from aqueous solution using new activated carbons developed from pomegranate peel: Adsorption equilibrium and kinetics, J. Hazard. Mater. 165 (2009) 52–62.